Published in final edited form as:

Cancer Discov. 2019 October ; 9(10): 1452–1467. doi:10.1158/2159-8290.CD-19-0298.

Altered nuclear export signal recognition as a driver of oncogenesis

Justin Taylor[1,2], **Maria Sendino**[3], **Alexander N. Gorelick**[1,4], **Alessandro Pastore**[1], **Matthew T. Chang**[1,4,†], **Alexander V. Penson**[1,4], **Elena I. Gavrila**[1,4], **Connor Stewart**[1], **Ella M. Melnik**[1], **Florisela Herrejon Chavez**[5], **Lillian Bitner**[1], **Akihide Yoshimi**[1], **Stanley Chun-wei Lee**[1], **Daichi Inoue**[1], **Bo Liu**[1], **Xiao J. Zhang**[1], **Anthony R. Mato**[2], **Ahmet Dogan**[6], **Michael G. Kharas**[5], **Yuhong Chen**[7], **Demin Wang**[7], **Rajesh K. Soni**[8,††], **Ronald C. Hendrickson**[8], **Gorka Prieto**[9], **Jose A. Rodriguez**[3], **Barry S. Taylor**[1,4,10], **Omar Abdel-Wahab**[1,2,11,*]

[1]Human Oncology and Pathogenesis Program, Memorial Sloan Kettering Cancer Center, New York, NY, USA.

[2]Leukemia Service, Department of Medicine, Memorial Sloan Kettering Cancer Center, New W, York, NY, USA.

[3]Department of Genetics, Physical Anthropology and Animal Physiology, University of the Basque Country, Barrio Sarriena s/n, Leioa, Spain.

[4]Department of Epidemiology and Biostatistics, Memorial Sloan Kettering Cancer Center, New York, NY, USA.

[5]Molecular Pharmacology Program, Memorial Sloan Kettering Cancer Center, New York, NY, USA

[6]Department of Pathology, Memorial Sloan Kettering Cancer Center, New York, NY, USA.

[7]Blood Research Institute, Blood Center of Wisconsin, Milwaukee, WI, USA.

[8]Microchemistry and Proteomics Core Facility, Memorial Sloan Kettering Cancer Center, New York, NY, USA.

[9]Department of Communications Engineering, University of the Basque Country (UPV/EHU), Bilbao 48013, Spain.

[10]Marie-Josée and Henry R. Kravis Center for Molecular Oncology, Memorial Sloan Kettering Cancer Center, New York, NY, USA.

[*]Correspondence: Omar Abdel-Wahab, 1275 York Ave. New York, NY 10065, Tel: 646-888-3487 Fax: 646-422-0298, abdelwao@mskcc.org.

AUTHOR CONTRIBUTIONS

Conceptualization: J.T., J.-A.R., B.S.T., O.A.-W. Data Curation: J.T., B.S.T. Formal Analysis: J.T., A.G., A.P., M.T.C., A.V.P., E.I.G., C.S., R.K.S., R.C.H., G.P., B.S.T., J.-A.R. Funding acquisition: J.T., O.A.-W. Investigation: J.T., M.S., A.G., A.P., A.V.P., C.S., E.M., F.H.C., L.B., A.Y., S.C.L., D.I., B.L., X.J.Z., A.M., A.D., Y.C., D.W., R.K.S., R.C.H., G.P., J.-A.R, B.S.T. Project Administration: J.T., J.-A.R., B.S.T., O.A.-W.. Resources: J.T., M.S., G.P., J.-A.R., O.A.-W. Supervision: M.G.K., D.W., R.C.H., J.A.-R., B.S.T., O.A.-W. Validation: J.T. Visualization: J.T., A.G., A.P., R.K.S., G.P., J.-A.R., B.S.T., O.-A.W.. Writing- original draft: J.T., O.A.-W. Writing- review & editing: J.T., A.Y., S.C.L., D.I., G.P., B.S.T., J.-A.R., O.A.-W.

[†]Current address: Genentech Inc., South San Francisco, CA

[††]Current address: Proteomics Core, Herbert Irving Comprehensive Cancer Center, Columbia University Medical Center, New York, USA

Conflict of interest disclosure: O.A.-W. has served as a consultant for H3B Biomedicine, Foundation Medicine Inc, Merck, and Janssen; O.A.-W. has received prior research funding from H3B Biomedicine unrelated to the current manuscript.

[11]Lead Contact

Abstract

Altered expression of XPO1, the main nuclear export receptor in eukaryotic cells, has been observed in cancer and XPO1 has been a focus of anti-cancer drug development. However, mechanistic evidence for cancer-specific alterations in XPO1 function is lacking. Here, genomic analysis of 42,793 cancers identified recurrent and previously unrecognized mutational hotspots in *XPO1.* XPO1 mutations exhibited striking lineage specificity, with enrichment in a variety of B-cell malignancies, and introduction of single amino acid substitutions in XPO1 initiated clonal, B-cell malignancy *in vivo*. Proteomic characterization identified that mutant XPO1 altered the nucleo-cytoplasmic distribution of hundreds of proteins in a sequence-specific manner that promoted oncogenesis. XPO1 mutations preferentially sensitized cells to inhibitors of nuclear export, providing a biomarker of response to this family of drugs. These data reveal a new class of oncogenic alteration based on change-of-function mutations in nuclear export signal recognition and identify therapeutic targets based on altered nucleo-cytoplasmic trafficking.

Keywords

Chronic lymphocytic leukemia (CLL); CRM1; Diffuse large B cell lymphoma (DLBCL); exportin-1; Hodgkin lymphoma; IκBα; Lymphoma; NF-κB; selinexor; XPO1

Introduction

Proper nucleocytoplasmic partitioning of macromolecules is essential to cellular homeostasis and is regulated by the nuclear pore complex and transport proteins that mediate trafficking of molecules across the nuclear envelope. Exportin-1 (XPO1; previously known as CRM1) is the major nuclear export receptor for proteins larger than ~40 kDa. To perform its exporting function, XPO1 identifies signals known as nuclear export signals (NESs) embedded in the amino acid sequence of cargo proteins. Protein cargoes bind XPO1 in the nucleus cooperatively with the small GTPase Ran, and the formation of ternary XPO1-RanGTP-cargo complexes begins the export process (1-3).

Numerous cellular pathways are regulated by controlling the subcellular localization of intermediate signaling proteins. Mutations that alter this nucleo-cytoplasmic localization in *cis* have been shown to drive transformation in a number of cancers (4-8). For example, mutations in nucleophosmin 1 (NPM1) that generate an NES and result in aberrant NPM1 cytoplasmic localization are among the most common genetic alterations in acute myeloid leukemia (9, 10). Similarly, mutations generating or eliminating an NES in BRCA1(11), VHL(12), and other recurrently mutated genes in cancer have been described. In addition, alterations in the machinery regulating nuclear export globally have been observed in cancer. Notably, increased expression of XPO1 has been described in numerous cancers (13-16), and many clinical trials have studied the efficacy of drugs inhibiting XPO1 in cancer patients (16-21).

Despite interest in XPO1 as a therapeutic target in cancer, mechanistic evidence for cancer-specific derangements in XPO1 function has not been demonstrated. Mutations in *XPO1* occur in a variety of cancers (22-25), but the functional contributions of these mutations to tumorigenesis are also unknown. Further, there are no biomarkers of response to XPO1 inhibitors in advanced-phase clinical trials. Given that XPO1 is an essential protein in eukaryotic cells, defining biomarkers of response may define patients most likely to respond to these agents and potentially limit toxicity. Here, we find that *XPO1* mutations are positively selected for in a variety of cancers and sensitize cells to XPO1 inhibitors. Specific mutant residues in XPO1 directly promote malignant transformation by altering the ability of XPO1 to engage protein cargo for nuclear export. These data identify a novel model of oncogenesis: tumorigenesis driven by mutations that change the global distribution of proteins across the nuclear membrane. In addition, these data implicate mutant XPO1, as well as its consequently mis-trafficked protein cargo, as targets for anti-cancer therapy.

Results

XPO1 mutations are recurrent across cancers and exhibit lineage specificity

Recent genomic analyses have identified recurrent heterozygous *XPO1* E571 mutations in a variety of cancer types, including chronic lymphocytic leukemia (CLL) (22, 23), Hodgkin's lymphoma (HL) (24), and esophageal carcinoma (25), among others. To systematically quantify the frequency and significance of *XPO1* mutational hotspots, we performed a large-scale analysis of whole-exome and genome sequencing data from 42,793 cancer patients spanning 322 cancer types, using an extensively validated computational framework (26, 27). We identified highly recurrent and statistically significant hotspots in *XPO1* at E571 (n = 99 patients; q-*value* = 10^{-204}), D624 (n = 6 patients; q-*value* = 10^{-11}), and R749 (n = 21 patients; q-*value* = 10^{-22}) residues (Fig. 1A), the latter two hotspots being previously unidentified. In addition, we found remarkable lineage-specificity of *XPO1* hotspot mutations. E571K, the most common *XPO1* mutation, was enriched in B-cell lymphomas, including primary mediastinal B-cell lymphoma (PMBL, 33%) , classical HL (14%), and diffuse large B-cell lymphoma (DLBCL, 2%), and in CLL (3%) (Fig. 1B and C; Supplementary Fig. S1A). In contrast, *XPO1* D624 mutations were found only in CLL while those at R749 were found mostly in non-lymphoid solid tumor malignancies (Supplementary Table S1). Strikingly, *XPO1* mutations were only found in the heterozygous state and never occurred as homozygous or hemizygous (i.e., loss-of-heterozygosity) mutations. We confirmed this in a separate cohort of 2,877 patients with hematologic malignancies in which we analyzed both mutations as well as copy-number state of *XPO1.* We found only a single patient who had both mutation as well as copy number alteration in *XPO1* (a gain of mutant XPO1). Even in this case the wild-type (WT) *XPO1* allele was retained (Supplementary Fig. S1B). These findings altogether suggest a novel change-of-function in *XPO1* caused by mutation.

XPO1^{E571K} mutation promotes growth of established malignant B cells

The recurrence, more often than expected in the absence of selection, of mutations at specific amino acid residues in XPO1 suggests that *XPO1* hotspot mutations functionally promote B-cell malignancies and other cancers. To evaluate the functional effects of *XPO1*

mutations, we used genome editing to generate isogenic B-cell leukemia cells (NALM-6 cells (28)) with physiologic expression of the *XPO1*^{E571K} mutation from the endogenous *XPO1* locus (Supplementary Fig. S1C). There was an equal ratio of *XPO1* E571K mutant allele to WT allele at the level of genomic DNA and mRNA (50% variant allele frequency). Expression of the heterozygous *XPO1*$^{E571K/WT}$ mutation in NALM-6 cells resulted in increased proliferation *in vitro* in both non-competitive and competitive growth assays relative to *XPO1* WT counterparts (Supplementary Fig. S1D-F). Enhanced growth of *XPO1*$^{E571K/WT}$ mutant cells was also seen *in vivo* through xenotransplantation of equal numbers of luciferase-labeled *XPO1*$^{E571K/WT}$ mutant or *XPO1*$^{WT/WT}$ cells (Fig. 1D and E; Supplementary Fig. S1G). The effects of *XPO1* mutation were distinct from *XPO1* genetic depletion, which completely suppressed cell growth (Supplementary Fig. S1D), a finding consistent with the known essentiality of XPO1 for cell survival (29, 30).

Xpo1^{E571K} mutations promote B-cell proliferation and transformation *in vivo*

Given the high conservation of XPO1 across mammals (Supplementary Fig. S2A), we next generated a conditional knock-in mouse model to express the *Xpo1*^{E571K} mutation from the endogenous *Xpo1* locus to determine its *in vivo* effects (Supplementary Fig. S2B-C). Heterozygous expression of *Xpo1*^{E571K} in the B-cell compartment using *CD19*-cre *Xpo1*$^{E571K/WT}$ mice resulted in selective expression of the *Xpo1*^{E571K} mutation in B cells at approximately 50% allelic ratio and had no effect on XPO1 protein expression in B cells relative to Cre-negative *Xpo1*$^{E571K/WT}$ controls (Supplementary Fig. S2D-F).

CD19-cre *Xpo1*$^{E571K/WT}$ mice were born at expected Mendelian ratios (Supplementary Fig. S3A) but were smaller in bodyweight relative to littermate controls (Supplementary Fig. S3B). Despite the smaller body size, *CD19*-cre *Xpo1*$^{E571K/WT}$ mice had significantly larger spleens at 12-weeks of age (Fig. 1F) Colony forming assays in IL-7 using bone marrow (BM) from mice with tamoxifen-inducible pan-hematopoietic *Xpo1*$^{E571K/WT}$ expression (*CAG*-creERT *Xpo1*$^{E571K/WT}$ mice) revealed increased numbers of B-cell colonies with enhanced clonogenicity upon replating (Fig. 1G), a finding restricted to the B-cell compartment (Supplementary Fig. S3C) and lost in the absence of IL-7 supplementation (Supplementary Fig. S3D). *CD19*-cre *Xpo1*$^{E571K/WT}$ mice died more rapidly than littermate controls and had increased B-cell proliferation, B-cell lymphocytosis, anemia, and thrombocytopenia (Fig. 2A; Supplementary Fig. S3E-H), and had increased numbers of mature ($CD19^+$ IgM^+ IgD^+) B cells in the BM and transitional T1, T2 B cells ($CD19^+$ $CD21^{lo}$ IgM^{hi} $CD93^+$ $CD23^-$ and $CD19^+$ $CD21^{lo}$ IgM^{hi} $CD93^+$ $CD23^+$, respectively) in the spleen as well as splenomegaly (Fig. 2B-D). *CD19*-cre *Xpo1*$^{E571K/WT}$ mice developed greater splenomegaly (Fig. 2E) as a result of increased generation of germinal centers and germinal center ($B220^+$ FAS^+ $GL7^+$) B cells upon allo-immunization with sheep red blood cells (SRBC), an effect which was evident 7 days after a single SRBC injection (Fig. 2F; Supplementary Fig. S3I **and** S3J).

A portion of *CD19*-cre *Xpo1*$^{E571K/WT}$ mice developed a lethal B-cell disease infiltrating lymph nodes, spleen, lungs, and BM, with co-expression of CD5 and CD23, characteristic features of human CLL, a cancer type frequently carrying *XPO1* E571 mutations (Fig. 2G; Supplementary Fig. S4A-E). Next-generation sequencing of VDJ sequences from splenic

mononuclear cells of these mice at the time of death identified productive clonal sequences occupying >98% of the total reads, indicating the presence of a highly clonal B-cell malignancy (Supplementary Fig. S4F).

Xpo1^{E571K} mutations promote lymphomagenesis driven by c-MYC and BCL-2

The above data reveal that expression of cancer-associated *XPO1* mutations can initiate lymphomagenesis when the correct microenvironmental stimulus is present (alloantigen from SRBC immunization). However, more aggressive lymphomas featuring *XPO1* E571K mutations may require additional cooperating mutations to fully manifest the disease phenotype. To evaluate this hypothesis, we crossed *Xpo1*$^{E571K/WT}$ mice to mice with overexpression of either c-MYC (using the *Eμ*–Myc mouse model (31)) or BCL2 (using *Vav*-BCL2 transgenic mice (32)) to model the aggressive lymphomas marked by overexpression of either of these oncogenic proteins in addition to *XPO1* mutations.

First, we crossed *Eμ*–Myc mice (which express human c-MYC transgenically from the immunoglobulin locus) to *CAG*-creERT *Xpo1*$^{E571K/WT}$ mice, allowing induction of mutant *XPO1* only after exposure to tamoxifen (Fig. 3A; Supplementary Fig. S5A). Mice transplanted with *Eμ*-Myc driven lymphomas conditionally expressing *Xpo1*$^{E571K/WT}$ in hematopoietic cells following engraftment (*CAG*-creERT *Xpo1*$^{E571K/WT}$ *Eμ*–Myc mice exposed to tamoxifen) succumbed to lethal disease more rapidly than controls (*CAG*-creERT *Xpo1*$^{E571K/WT}$ *Eμ*–Myc mice exposed to vehicle; Fig. 3B and C). Expression of *Xpo1*$^{E571K/WT}$ further increased B-cell lymphocytosis driven by *Eμ*–Myc throughout the blood, spleen, and BM, resulting in more rapidly lethal spleen and BM infiltration (Fig. 3D-F). Here again, sequencing of VDJ sequences from splenic mononuclear cells confirmed that death was due to infiltration of B-cells which were >90% clonal (Supplementary Fig. S5B). Notably, a subset of the B-cells gained aberrant CD5 expression (Supplementary Fig. S5C) and *Eμ*–Myc *CAG*-creERT *Xpo1*$^{E571K/WT}$ mutant cells were larger as measured by flow cytometry as well as cytologic analysis with Wright-Giemsa stain compared to controls (Supplementary Fig. S5D-E). Whole transcriptomic analysis by mRNA sequencing (RNA-seq) of tumors from *CAG*-creERT *Xpo1*$^{E571K/WT}$ *Eμ*–Myc and *CAG*-creERT *Eμ*–Myc controls revealed Xpo1E571K expression in the context of *Eμ*–Myc tumors increased expression of established MYC targets as well as gene expression programs related to cell cycle, nuclear export, and NF-κB activation (Fig. 3G).

Next, we crossed *Vav*-BCL2 transgenic mice (which overexpress human BCL2 throughout the hematopoietic system) to *CD19*-cre *Xpo1*$^{E571K/WT}$ mice (Fig. 4A). *CD19*-cre *Xpo1*$^{E571K/WT}$ *Vav*-BCL2 mice had increased peripheral blood leukocytosis, splenomegaly, and a greater absolute number of B cells in the blood, BM, and spleen compared to *CD19*-cre *Vav*-BCL2 controls (Fig. 4B; Supplementary Fig. S6A **and** S6B). *In vivo* bromodeoxyuridine (BrdU) uptake assays also confirmed that mice with combined *Xpo1* mutation and BCL2 overexpression had greater splenomegaly and higher numbers and proliferation of BM and splenic B cells relative to controls (Fig. 4C-D; Supplementary Fig. S6C). *In vitro* proliferation and self-renewal (measured by colony-forming assays in IL-7) was also greater in *CD19*-cre *Xpo1*$^{E571K/WT}$ *Vav*-BCL2 than in *CD19*-cre *Xpo1*$^{WT/WT}$ *Vav*-BCL2 mice (Fig. 4E). Overall, *CD19*-cre *Xpo1*$^{E571K/WT}$ *Vav*-BCL2 mice had increased B-

cell invasion in the spleen, BM, and lungs (Fig. 4F) and succumbed to lethal B-cell malignancy sooner than controls (Supplementary Fig. S6D). Gene set enrichment analysis of genes differentially expressed between *CD19*-cre *Xpo1*$^{E571K/WT}$ *Vav*-BCL2 and *CD19*-cre *Xpo1*$^{WT/WT}$ *Vav*-BCL2 mice was significant for receptor cytokine signaling via NF-κB, a pattern that was seen in the *CD19*-cre *Xpo1*$^{E571K/WT}$ versus WT mice in the absence of BCL2 (Fig. 4G).

Altered nuclear/cytoplasmic compartmentalization of proteins in *XPO1*^{E571K} mutant cells

To evaluate how mutations in *XPO1* might drive lymphoid malignancy development, we next sought to identify patterns of mutational co-occurrence or exclusivity in patients bearing XPO1 E571K mutations. In an additional cohort of 2,877 patients with hematologic malignancies who were uniformly sequenced by the MSK HemePACT assay (33), we identified 29 XPO1 mutant patients from patients with CLL (n=288), HL (n=16), PMBL (n=9), B-cell acute lymphoblastic leukemia (n=142), or DLBCL (n=284). While we identified numerous genetic alterations co-existing with *XPO1* mutations in each of these histologic subtypes of B-cell malignancies (Supplementary Fig. S7A-D), there were no statistically different mutational co-occurrences between *XPO1* mutant versus WT cases in each of these disease categories. We also similarly sequenced a cohort of splenocytes at time of death from three *CD19*-cre *Xpo1*$^{E571K/WT}$ mice and three *CD19-cre Xpo1*$^{WT/WT}$ mice of similar age (using a sequencing panel targeting the entire coding region of the mouse orthologs of 578 genes recurrently mutated in solid tumors, lymphomas, and leukemias (Supplementary Table S2)). This revealed several somatic mutations in one of the three *CD19*-cre *Xpo1*$^{E571K/WT}$ mice including compound p53 mutations (Trp53Y120S, TrpM157V), an Msh2 splice site mutation (*Msh2* c.793–8A>T), and a missense mutation in *Tcf7l2* (Tcf7l2S512L), a transcription factor through which β-catenin functions.

Given the known role of XPO1 in nuclear export, we next took an unbiased proteomics approach to detect pathways and individual XPO1 cargoes impacted by the E571K mutation. We quantified the partitioning of proteins between the cytoplasm and nucleus of human B-cell malignant cells (NALM-6 cells) with or without knock-in of *XPO1*$^{E571K/WT}$. We performed SILAC (stable isotope labeling with amino acids in cell culture)-based mass spectrometry on fractionated nuclear and cytoplasmic lysates from *XPO1*$^{E571K/WT}$ and *XPO1*$^{WT/WT}$ NALM-6 cells (Fig. 5A). Several proteins were identified as significantly differentially exported in *XPO1*$^{E571K/WT}$ versus *XPO1*$^{WT/WT}$ cells (fold change ratios >|2| and $-\log_{10}$[*P*-value] ≥ 1.30; Fig. 5B; Supplementary Tables S3-5), including numerous members of the K63-ubiquitination, TLR4, and NF-κB pathways, among others (Fig. 5C).

Phenotypically, *XPO1*$^{E571K/WT}$ cells demonstrated higher baseline and post-activation NF-κB and NFAT transcriptional responses to stimulation with TNF-α or PMA/ionomycin, respectively, than *XPO1*$^{WT/WT}$ cells (Fig. 5D and E). Differential gene expression analysis of mRNA-sequencing of pro-B ($CD19^+$ $CD43^+$ $CD24^+$ BP-1^-), pre-B ($CD19^+$ $CD43^-$ IgM^- IgD^-), immature ($CD19^+$ $CD43^-$ IgM^+ IgD^-), and mature B cells ($CD19^+$ $CD43^-$ IgM^+ IgD^+) from *CD19*-cre *Xpo1*$^{E571K/WT}$ and littermate *CD19*-cre *Xpo1*$^{WT/WT}$control mice identified prominent upregulation of pathways associated with cytokine signaling and immune responses in *Xpo1*$^{E571K/WT}$ mutant mature B-cells relative to controls (Fig. 5F;

Supplementary Fig. S8A-B). Consistent with this finding, serum from 12-week-old *CD19*-cre *Xpo1*$^{WT/WT}$ and *CD19*-cre *Xpo1*$^{E571K/WT}$ mice contained increased IgM auto-antibodies to histone H1, a finding associated with dysregulated immune signaling (Supplementary Fig. S8C). Moreover, we identified a similar transcriptional signature of increased cytokine immune response and inflammation in human CLL patients with *XPO1* mutations compared to CLL patients without *XPO1* mutations (Fig. 5G; Supplementary Table S6). Differential export of NF-κB and NFAT signaling proteins was confirmed by western blot, which revealed enhanced nuclear phosphorylated p65 and NFAT2 in XPO1 mutants relative to wild-type (Fig. 5H and I). Other proteins whose subcellular localization was altered by *XPO1*$^{E571K/WT}$ in our SILAC experiment were confirmed by western blot, including TRAF2 (increased in nuclear export in the setting of mutant XPO1E571K) and p120 catenin (which was decreaed in nuclear export in the setting of mutant XPO1 E571K; Supplementary Fig. S8D). Finally, the increased NF-κB and NFAT signaling and differential export of their member proteins by *XPO1*$^{E571K/WT}$ were validated in a CLL cell line (MEC1) engineered to express WT or E571K mutant XPO1 as well as a series of mature B cell lymphoma cell lines naturally carrying endogenous XPO1 E571K mutations (Supplementary Fig. S8D-H).

XPO1^{E571K} mutations are predicted to alter the function of XPO1 nuclear export

XPO1 binds to its cargo by recognizing 8 to 15 residue amino acid motifs known as leucine-rich NESs (1-3, 34), which show a characteristic spacing of hydrophobic residues separated by other amino acids (described as Φ^1-$X_{(2,3)}$- Φ^2-$X_{(2,3)}$-Φ^3-X-Φ^4 where "Φ" represents leucine, isoleucine, valine, phenylalanine, or methionine). Atomic-level characterization of the XPO1/ NES interaction has revealed that XPO1 binds NES of cargo proteins in a hydrophobic cleft on the outer convex surface of XPO1 (35-38). We therefore modeled the position of *XPO1* hotspot mutations on the three-dimensional structure of XPO1 to understand the mechanism by which these mutations alter nuclear export of the proteins we identified. Interestingly, the two hotspot mutations in *XPO1* arising in CLL and B-cell lymphomas (D624 and E571), although separated in two-dimensional amino acid sequence, were both adjacent in the cognate folded protein structure of the NES binding cleft of XPO1 (Fig. 6A). Further structural modeling predicted that the change of a negatively charged glutamic acid at XPO1 E571 to a positively charged lysine would promote XPO1 interaction with protein cargo bearing negatively charged amino acid residues C-terminal to the NES (Fig. 6B). Simultaneously, XPO1 E571K mutation would be predicted to repel interactions with proteins bearing amino acids that have positively charged amino acids C-terminal to the NES.

XPO1^{E571K} mutations alter NES recognition in a sequence-specific manner

As described above, analysis of our SILAC-based mass spectrometry data identified a number of NES-bearing proteins as depleted in the nucleus and/or enriched in the cytoplasm of *XPO1*$^{E571K/WT}$ mutant versus *XPO1*$^{WT/WT}$ cells beyond NF-κB and NFAT proteins. Analysis of the amino acid sequence of these proteins with an NES prediction tool (39) identified several putative NESs in these proteins in addition to the known NESs. In proteins showing enhanced export by mutant XPO1, the proportion of predicted NESs with a negative net charge in their C-terminal end were more frequent (Fig. 6C-D). Conversely,

proteins showing reduced export by mutant XPO1, more frequently had NESs with a net positive charge in their C-terminal end.

We utilized a cellular reporter containing one of the NESs to evaluate the sequence-specific effects of XPO1 hotspot mutations on nuclear export, which were suggested by the structural and proteomic analyses above. We used a modified version of a previously described nuclear export reporter (40) where the first 100 amino acids of the XPO1 substrate Survivin (bearing its NES) are fused to a 3X FLAG epitope and two nuclear localization signals (Supplementary Fig. S9A). We generated three versions of this reporter: (1) the native NES, (2) a mutant NES where amino acids C-terminal to the last hydrophobic residue were enriched in positive charges, and (3) a mutant version where amino acids C-terminal to the last hydrophobic residue were enriched in negative charges. Co-transfection of each of these 3 NES reporters with either WT or E571K mutant XPO1 revealed that the XPO1 E571K mutant significantly enhanced export of the negatively charged NES construct, while reducing export of the positively charged NES construct (Fig. 6E-G; Supplementary Fig. S9B-C). We validated these findings with a second reporter based on the HIV Rev protein NES (the Rev(1.4)-GFP reporter (41) with insertion of the IκBα NES) with an additional step of adding cycloheximide to inhibit new protein translation in the cytoplasm (Supplementary Fig. S9D). This experiment, once again, revealed that XPO1 E571K mutant greatly enhanced nuclear export of negatively charged NES. Overall, these experiments confirmed that XPO1 E571K alters nuclear export on the basis of the charge properties of amino acids surrounding the NES of XPO1 cargo proteins (Supplementary Fig. S9E-F). Interestingly, the XPO1 D624G hotspot mutation was predicted to disrupt hydrogen bonding between XPO1 and cargo protein at a site further removed from the NES (Supplementary Fig. S10A). Consistent with this prediction, the XPO1 D624G mutation decreased export compared to XPO1 WT, a finding which was not altered by changing the C-terminal sequence of the NES (Supplementary Fig. S10B-C).

XPO1 mutant cells are preferentially sensitive to XPO1 inhibition

Inhibitors of nuclear export that bind to the cysteine 528 residue of XPO1 and occupy the NES-binding pocket of XPO1, thereby blocking XPO1 function, have recently been tested in phase 2 and 3 clinical trials. The XPO1 inhibitor compound selinexor recently received Orphan Drug and Fast Track FDA designation for relapsed multiple myeloma. However, biomarkers of response to XPO1 inhibition are not known, and it is not known if cancer-associated mutations in XPO1 modify response to XPO1 inhibitors. Interestingly, leukemia or lymphoma cells with naturally occurring *XPO1*^{E571K} mutations were among the most sensitive to the XPO1 inhibitor KPT-185 across 75 cell lines in publicly available cell line dependency data (depmap.org; Supplementary Fig. S11A). This finding was also seen in *XPO1*^{E571K} mutant B-cell lymphoma cell lines exposed to selinexor compared to those WT for *XPO1* (Supplementary Fig. S11B) where *XPO1*^{E571K} mutant cell lines were all more sensitive to selinexor compared to WT cells. The enhanced sensitivity of XPO1^{E571K} mutant cells to selinexor were further seen in isogenic human B-cells (NALM-6 cells), B-cells from *CD19*-cre *Xpo1*$^{E571K/WT}$ knock-in mice, and mice with combined *Xpo1*^{E571K} mutation and BCL2 overexpression relative to *XPO1*^{WT} counterparts *in vitro* (Fig. 7A-C). Similar enhanced sensitivity of XPO1 mutant cells to selinexor was seen *in vivo*: selinexor extended

the survival of mice bearing *Eμ*-Myc *Xpo1*^{E571K} mutant lymphomas compared to vehicle to a far greater extent than in mice bearing *Eμ*-Myc *Xpo1*^{WT} lymphomas (Fig. 7D; Supplementary Fig. S11C). Selinexor also decreased the spleen size and percentage of CD5^{+} B-cells in the spleen of secondary recipients engrafted with CLL cells from *CD19*-cre *Xpo1*$^{E571K/WT}$ mice (Supplementary Fig. S11D-F).

To evaluate the basis for preferential effects of XPO1 inhibition on cells bearing cancer-associated *XPO1* hotspot mutations, we next assessed XPO1 protein abundance and nuclear/cytoplasmic protein compartmentalization by *XPO1* mutant genotype in the context of XPO1 inhibition. Interestingly, selinexor treatment resulted in enhanced dose-dependent degradation of XPO1 in *XPO1* mutants relative WT cells (Fig. 7E). The close proximity of the XPO1 E571 residue to the known binding residue of selinexor on XPO1 at C528 (Supplementary Fig. 11G) suggested that the XPO1 E571K mutation might influence the binding affinity of XPO1 inhibitors to the mutant XPO1 protein. Consistent with this prediction, microscale thermopheresis assays with the XPO1 inhibitor, KPT-185, identified that the XPO1 E571K mutant protein bound KPT-185 with greater affinity than XPO1 WT protein (Fig 7F; Supplementary Fig. S11H). Within cells, XPO1 inhibition resulted in preferential degradation of the XPO1 E571K protein as identified in MEC1 cells expressing XPO1 WT or E571K FLAG-tagged protein treated with selinexor (Supplementary Fig. S12A). Finally, proteomic analysis by tandem mass tag mass spectrometry of cells treated with XPO1 inhibitor compared to vehicle also revealed mutant-selective changes in the localization of many proteins after XPO1 inhibition (Supplementary Fig. S12B-C). Certain proteins, including p53, while retained in the nucleus upon XPO1 inhibition in both WT and mutant cells, were retained at higher levels in *XPO1*^{E571K} mutant cells (Supplementary Fig. S12D). However, other proteins had increased nuclear retention upon XPO1 inhibition only in *XPO1*^{E571K} cells, suggesting potential synthetic lethal interactions. These proteins included members of critical cell pathways such as cell-cycle, translation, mRNA splicing, and innate immune signaling (Fig. 7G).

Discussion

Our data present a novel model of tumorigenesis: change-of-function mutations in nucleo-cytoplasmic trafficking machinery driving transformation. Systematic quantification of *XPO1* mutations across large-scale sequencing data from numerous cancer types enabled the identification of specific hotspot mutations in *XPO1* as among the most common mutations in patients with CLL, HL, and PMBL, showing lineage specificity and occurring as heterozygous point mutations. Prior work suggests that XPO1 mutations in CLL are clonal at diagnosis and likely to be present at relapse as well, suggesting an early founder mutation (23). Consistent with this notion, XPO1 E571 mutations have been tracked in plasma cell-free DNA in patients with HL (24), where their presence correlates with tumor regression or progression and the frequency of XPO1 mutations in CLL does not appear to be significantly different between the treatment-naïve or relapsed/refractory state (42).

While the discovery of hotspot mutations in *XPO1* suggests an oncogenic driver function, XPO1 is expressed in every eukaryotic cell and is essential for cell survival. The essential housekeeping function of XPO1 has presented a barrier to manipulating endogenous XPO1

in vivo. Consequently, there has never been an animal model of any alteration in XPO1 previously. Here, we overcame this technical challenge and identified that a single amino acid substitution in Xpo1 *in vivo* increased B-cell proliferation and resulted in the development of clonal B-cell malignancies resembling human CLL. These models thereby provide one of the few genetically accurate murine models of CLL and establish the causality of XPO1 mutations in cancer development. Moreover, expression of the $Xpo1^{E571K}$ mutation *in vivo* also promoted development of other types of B-cell malignancies in concert with oncogenes such as MYC and BCL2.

The biochemical, structural, proteomic, and molecular studies here indicate that XPO1 mutations alter nuclear export recognition in a sequence-specific manner, favoring the export of cargoes with negatively charged C-terminus NES sequences as a result of changes in charge near the NES binding cleft of XPO1. The generation of genetic models of mutant XPO1 enabled us to characterize the malignant mutant XPO1 exportome. Hundreds of proteins in various pathways were affected by altered NES recognition by mutant XPO1, including changes in the nucleo-cytoplasmic distribution of proteins involved in inflammatory signaling, DNA repair, RNA export, and chromatin remodeling pathways. While it might be expected that the abundance of individual proteins detected in nuclear and cytoplasmic fractions would yield symmetrical results with proteins enriched in nuclear analysis showing up as depleted in the cytoplasmic fraction and vice versa, this was not seen here or in prior analyses (43-45). In contrast, the vast majority of shuttling proteins assayed by mass spectrometric analysis of nuclear and cytoplasmic fractions show changes in only one cellular compartment without the expected reciprocal change in the other compartment. Potential explanations for this lack of overlap include the fact that many proteins are exported from the nucleus as part of their regulation and are degraded after nuclear export. Additionally, the balance between nuclear export and import is important and changing nuclear localization could result in changes in protein stability.

Drugs that inhibit XPO1 binding to cargo proteins have been demonstrated to have therapeutic efficacy for a number of cancer types (18-21, 46). As a result, altered function of XPO1 has been suggested to be common in cancer, but there has been no demonstration of XPO1 driving tumor development previously. The genomic data from patients as well as these functional data show that *XPO1* mutations are selected for in cancer cells and promote malignant transformation by altering activation of pathways such as NF-κB and NFAT signaling. This discovery that mutant XPO1 can functionally drive tumorigenesis may be particularly useful for the development of targeted therapies for malignancies bearing XPO1 hotspot mutations; indeed, $XPO1^{E571K}$ was associated with increased sensitivity to XPO1 inhibitors currently in clinical trials. Thus, these data establish oncogenic mutations in nuclear export machinery and identify these mutations as novel drivers of tumorigenesis and potential targets of anti-cancer therapy.

Methods

See also Supplementary Materials for additional details.

Animals

All animals were housed at Memorial Sloan Kettering Cancer Center (MSK). All animal procedures were completed in accordance with the Guidelines for the Care and Use of Laboratory Animals and were approved by the Institutional Animal Care and Use Committees at MSK. Generation and genotyping of the *Xpo1*$^{E571K/WT}$ are described below.

Xpo1$^{E571K/WT}$ mice on a pure C57BL/6 background were crossed to *CD19*-cre mice (47), tamoxifen-inducible *CAG*-creERT mice (48), *Eμ*-Myc transgenic mice (31), and/or *Vav*-BCL2 transgenic mice (32), each of which were also maintained on a pure C57BL/6 background.

Eight-week-old female CD45.1 C57BL/6J mice (the Jackson Laboratory) were used as recipients for bone marrow transplantation assays and 8-week-old female NSG mice (the Jackson Laboratory) were used for cell-line xenografting. Blood was collected by submandibular bleeding using heparinized microhematocrit capillary tubes (Thermo Fisher Scientific). For assessment of germinal center formation, age- and sex-matched C57BL/6J mice were immunized intraperitoneally at 8 to 12 weeks old with 0.5 mL of a 2% sheep red blood cell (SRBC) suspension in PBS (Cocalico Biologicals) or PBS as control. Automated peripheral blood counts were obtained using a ProCyte Dx Hematology Analyzer (IDEXX).

Generation of *Xpo1*$^{E571K/WT}$ conditional knock-in mice

An 8.4 kb genomic DNA used to construct the targeting vector was first subcloned from a positively identified B6 BAC clone (RP23: 123E19). The region was designed such that the long homology arm (LA) extends ~5.73 kb 5’ to the engineered LoxP site, and the short homology arm (SA) extends 2.15 kb 3’ to the insertion of the inverted mutant exon26. The mutant exon 26 (CGG→TGC) plus the flanking genomic sequences for correct splicing (saEx26*sd) was inserted in the reverse direction in intron 26–27 and is 153 bp downstream of exon 26, which is immediately followed by a Lox66 site. A Lox71 site was placed 5’ to the inverted saEx26*sd sequence. The FRT-flanked Neo cassette was inserted immediately upstream of the Lox71/Lox66 flanked inversion sequence. The targeting vector was confirmed by restriction analysis and sequencing after each modification. The boundaries of the 2 homology arms were confirmed by sequencing with P6 and T73 primers that read through both sides of the backbone vector into the genomic sequence. The FRT-Neo cassette was confirmed by sequencing with LAN1 and iNeoN2 primers that read from the 5’- and 3’-ends of the Neo cassette, respectively, into the inverted saEx26*sd (LAN1) and the genomic sequence (iNeoN2). saEx26*sd and its junction with the genomic sequence were sequencing confirmed with primer LAN1. LOX1 sequencing result confirmed the engineered single LoxP site upstream of exon 26.

The targeting vector was confirmed by restriction analysis and sequencing after each modification step. The boundaries of the 2 homology arms were confirmed by sequencing with P6 and T73 primers that read through both sides of the backbone vector into the genomic sequences. LAN1 and N2 primers read from the selection cassette into the inversion cassette (LAN1) and the 3’ end of the middle arm (N2). The 5’ LoxP site and the 5’ junction of genomic sequence/eGFP was confirmed by sequencing with Lox1 primer.

Primer GFP3 sequencing confirmed the remaining eGFP-T2A sequence and its 3' junction with the genomic sequence. Primers LAN1, mCherrySQ1 and IMBPSQ1 confirmed the entire inversion cassette sequence and its junctions.

Primers used for sequencing:

Primer P6:	5'- GAG TGC ACC ATA TGG ACA TAT TGT C-3'
Primer T73:	5'- TAA TGC AGG TTA ACC TGG CTT ATC G-3'
Primer LAN1:	5'- CCA GAG GCC ACT TGT GTA GC-3'
Primer N2:	5'- TTC CTC GTG CTT TAC GGT ATC G-3'
Primer EXPO LOX1:	5'- CCC CTA ACC GCT TCC TCA TCT TAA GG-3'
Primer EXPO SQ1:	5'- GAC CAC ATG AAG CAG CAC GAC TTC-3'

The targeting construct was linearized using AscI prior to electroporation into embryonic stem (ES) cells. After selection with G418 antibiotic, surviving clones were expanded for polymerase chain reaction (PCR) analysis to identify recombinant ES clones. Secondary confirmation of positive clones identified by PCR was performed by southern blotting analysis. DNA was digested with XbaI (External long arm) or EcoRV (Internal short arm), and electrophoretically separated on a 0.8% agarose gel. After transfer to a nylon membrane, the digested DNA was hybridized with a probe targeted against the 5' external region. DNA from a normal C57BL/6 (B6) mouse was used as WT control. Positive ES clones were expanded and microinjected into Balb/c blastocysts. Resulting chimeras with a high percentage black coat color were mated to C57BL/6 FLP mice (The Jackson Laboratory) to remove the Neo cassette, and subsequently to *CD19*-cre or *CAG*-creERT transgenic mice. Mice were backcrossed for six generations to C57BL/6 mice and tamoxifen was administered to 6-week-old mice at 12 μg/g intraperitoneally every other day for 3 doses (as previously described (49)).

Genotyping of *Xpo1*$^{E571K/WT}$ conditional knock-in mice

Tail DNA samples from positive mice were amplified by PCR using the LOX1 and SDL2 primers. This reaction amplifies a wild-type product 409 bp in size. The presence of a second PCR product 62 bp greater than the wild-type product indicates a positive LoxP PCR. After a 2-minute hot start at 94 °C the samples were run using the following conditions for 30 cycles: 94 °C for 30s, followed by 55 °C for 30s, and 72 °C for 1 min. The PCR product was run on a 2% gel with a 100 bp ladder as reference.

Primers for PCR Screening:

Forward Oligo:

LOX1: 5'- TGG CTA AAC CAG AGG AGG TAC TG −3'

Reverse Oligo:

SDL2: 5'- ATG GAG CCT ATT GCC CAA CAC AAC −3'

Cell lines

NALM-6 cells engineered to express *XPO1*$^{E571K/WT}$ from the endogenous locus were generated by Horizon Discovery using recombinant adeno-associated virus mediated

homologous recombination and cultured in RPMI medium with 10% fetal calf serum (FCS). MEC1 cells were purchased from DSMZ. SUDHL-5. SUDHL-6, SUDHL-16, L428 and SUP-HD1 cells were a generous gift from Dr. Laura Pasqualucci. All cell lines were tested for mycoplasm with the MycoAlert™ Mycoplasma Detection Kit (Lonsa) at time of receipt and before preparing stock aliquots for storage in liquid nitrogen. Cells were thawed and passaged no more than 10 times for all experiments performed. Validation of the XPO1 E571K mutation was performed by next-generation targeted capture sequencing and serial routine testing was performed by PCR and Sanger sequencing.

Primary patient samples

Studies were approved by the Institutional Review Board of MSK and conducted in accordance to the Declaration of Helsinki protocol. We obtained written informed consent from patients before primary human de-identified CLL samples derived from whole peripheral blood or BM mononuclear cells were utilized.

Statistical analysis

All data are presented as mean ± standard deviation, unless otherwise stated. The replicate for each experiment is stated in the figure legend or indicated in the figure. Statistical significance was determined by a two-sided Student's t-test and a P value of <0.05 was considered statistically significant. For non-normally distributed data, a non-parametric test (Kruskal-Wallis) was used, followed by multiple group comparisons using false-discovery rate (FDR). For Kaplan-Meier survival analysis, a Mantel-Cox log-ranked test was used to determine statistical significance. For offspring frequency analysis, a Chi-Square test was performed to test the difference between observed and expected frequencies from different genotypes. No blinding or randomization was used. Unless otherwise noted, all immunoblot quantitation and immunofluorescence image quantitation were representative of at least three biological replicates from independent experiments. Data were plotted using GraphPad Prism 7 software.

Supplementary Material

Refer to Web version on PubMed Central for supplementary material.

Acknowledgements:

Editorial support in the preparation of this manuscript was provided by Hannah Rice, ELS.

Financial support: J.T. is supported by the Conquer Cancer Foundation of the American Society of Clinical Oncology, the American Association for Cancer Research, the American Society of Hematology (ASH), the Robert Wood Johnson Foundation, and the NIH/NCI (1K08CA230319–01). C.S. is supported by an ASH HONORS award. A.Y. is supported by grants from the Aplastic Anemia and MDS International Foundation and the Lauri Strauss Leukemia Foundation. A.Y., S.C.-W.L., D.I., and O.A.-W. are supported by the Leukemia and Lymphoma Society. S.C.-W.L is supported by the NIH/NCI (K99 CA218896), the ASH Scholar Award, and the EvansMDS Young Investigator Award. B.S.T. is supported by grants from NIH/NCI (R01 CA207244, R01 CA204749, U54 OD020355), the American Cancer Society (RSG-15–067-01-TBG), the Anna Fuller Fund, and the Robertson Foundation. D.W. is supported by grants from the NIH/NIAID (AI079087) and NIH/NHLBI (R01 HL130724). M.S. and J.-A.R. are supported by grants from the Spanish Government MINECO-FEDER (SAF2014–57743-R), the Basque Country Government (IT634–13 grant and a predoctoral fellowship) and the University of the Basque Country (UFI11/20). O.A.-W. is supported by grants from NIH/NHLBI (R01 HL128239) and NIH/NCI (1 R01 CA201247–01A1), an MSK Steven Greenberg Lymphoma Research Award, the Geoffrey Beene Research Center of

MSK, and the Pershing Square Sohn Cancer Research Alliance. This work was also supported by P30 CA008748. Research supported AACR-Conquer Cancer Foundation of ASCO Young Investigator Award for Translational Cancer Research.

References

1. Stade K, Ford CS, Guthrie C, Weis K. Exportin 1 (Crm1p) is an essential nuclear export factor. Cell. 1997;90:1041–50. [PubMed: 9323132]
2. Fukuda M, Asano S, Nakamura T, Adachi M, Yoshida M, Yanagida M, et al. CRM1 is responsible for intracellular transport mediated by the nuclear export signal. Nature. 1997;390:308–11. [PubMed: 9384386]
3. Ossareh-Nazari B, Bachelerie F, Dargemont C. Evidence for a role of CRM1 in signal-mediated nuclear protein export. Science. 1997;278:141–4. [PubMed: 9311922]
4. Jeyasekharan AD, Liu Y, Hattori H, Pisupati V, Jonsdottir AB, Rajendra E, et al. A cancer-associated BRCA2 mutation reveals masked nuclear export signals controlling localization. Nat Struct Mol Biol. 2013;20:1191–8. [PubMed: 24013206]
5. Pauty J, Couturier AM, Rodrigue A, Caron MC, Coulombe Y, Dellaire G, et al. Cancer-causing mutations in the tumor suppressor PALB2 reveal a novel cancer mechanism using a hidden nuclear export signal in the WD40 repeat motif. Nucleic Acids Res. 2017;45:2644–57. [PubMed: 28158555]
6. Nakagawa M, Kameoka Y, Suzuki R. Nucleophosmin in acute myelogenous leukemia. N Engl J Med. 2005;352:1819–20; author reply −20.
7. Mariano AR, Colombo E, Luzi L, Martinelli P, Volorio S, Bernard L, et al. Cytoplasmic localization of NPM in myeloid leukemias is dictated by gain-of-function mutations that create a functional nuclear export signal. Oncogene. 2006;25:4376–80. [PubMed: 16501600]
8. Stommel JM, Marchenko ND, Jimenez GS, Moll UM, Hope TJ, Wahl GM. A leucine-rich nuclear export signal in the p53 tetramerization domain: regulation of subcellular localization and p53 activity by NES masking. EMBO J. 1999;18:1660–72. [PubMed: 10075936]
9. Falini B, Mecucci C, Tiacci E, Alcalay M, Rosati R, Pasqualucci L, et al. Cytoplasmic nucleophosmin in acute myelogenous leukemia with a normal karyotype. N Engl J Med. 2005;352:254–66. [PubMed: 15659725]
10. Brunetti L, Gundry MC, Sorcini D, Guzman AG, Huang YH, Ramabadran R, et al. Mutant NPM1 Maintains the Leukemic State through HOX Expression. Cancer Cell. 2018;34:499–512 e9. [PubMed: 30205049]
11. Rodriguez JA, Henderson BR. Identification of a functional nuclear export sequence in BRCA1. J Biol Chem. 2000;275:38589–96. [PubMed: 10991937]
12. Lee S, Neumann M, Stearman R, Stauber R, Pause A, Pavlakis GN, et al. Transcription-dependent nuclear-cytoplasmic trafficking is required for the function of the von Hippel-Lindau tumor suppressor protein. Molecular and cellular biology. 1999;19:1486–97. [PubMed: 9891082]
13. Kojima K, Kornblau SM, Ruvolo V, Dilip A, Duvvuri S, Davis RE, et al. Prognostic impact and targeting of CRM1 in acute myeloid leukemia. Blood. 2013;121:4166–74. [PubMed: 23564911]
14. Schmidt J, Braggio E, Kortuem KM, Egan JB, Zhu YX, Xin CS, et al. Genome-wide studies in multiple myeloma identify XPO1/CRM1 as a critical target validated using the selective nuclear export inhibitor KPT-276. Leukemia. 2013;27:2357–65. [PubMed: 23752175]
15. Akagi I, Okayama H, Schetter AJ, Robles AI, Kohno T, Bowman ED, et al. Combination of protein coding and noncoding gene expression as a robust prognostic classifier in stage I lung adenocarcinoma. Cancer Res. 2013;73:3821–32. [PubMed: 23639940]
16. Walker CJ, Oaks JJ, Santhanam R, Neviani P, Harb JG, Ferenchak G, et al. Preclinical and clinical efficacy of XPO1/CRM1 inhibition by the karyopherin inhibitor KPT-330 in Ph+ leukemias. Blood. 2013;122:3034–44. [PubMed: 23970380]
17. Abdul Razak AR, Mau-Soerensen M, Gabrail NY, Gerecitano JF, Shields AF, Unger TJ, et al. First-in-Class, First-in-Human Phase I Study of Selinexor, a Selective Inhibitor of Nuclear Export, in Patients With Advanced Solid Tumors. J Clin Oncol. 2016;34:4142–50. [PubMed: 26926685]

18. Gounder MM, Zer A, Tap WD, Salah S, Dickson MA, Gupta AA, et al. Phase IB Study of Selinexor, a First-in-Class Inhibitor of Nuclear Export, in Patients With Advanced Refractory Bone or Soft Tissue Sarcoma. J Clin Oncol. 2016;34:3166–74. [PubMed: 27458288]
19. Alexander TB, Lacayo NJ, Choi JK, Ribeiro RC, Pui CH, Rubnitz JE. Phase I Study of Selinexor, a Selective Inhibitor of Nuclear Export, in Combination With Fludarabine and Cytarabine, in Pediatric Relapsed or Refractory Acute Leukemia. J Clin Oncol. 2016;34:4094–101. [PubMed: 27507877]
20. Garzon R, Savona M, Baz R, Andreeff M, Gabrail N, Gutierrez M, et al. A phase 1 clinical trial of single-agent selinexor in acute myeloid leukemia. Blood. 2017;129:3165–74. [PubMed: 28336527]
21. Kuruvilla J, Savona M, Baz R, Mau-Sorensen PM, Gabrail N, Garzon R, et al. Selective inhibition of nuclear export with selinexor in patients with non-Hodgkin lymphoma. Blood. 2017;129:3175–83. [PubMed: 28468797]
22. Puente XS, Pinyol M, Quesada V, Conde L, Ordonez GR, Villamor N, et al. Whole-genome sequencing identifies recurrent mutations in chronic lymphocytic leukaemia. Nature. 2011;475:101–5. [PubMed: 21642962]
23. Landau DA, Carter SL, Stojanov P, McKenna A, Stevenson K, Lawrence MS, et al. Evolution and impact of subclonal mutations in chronic lymphocytic leukemia. Cell. 2013;152:714–26. [PubMed: 23415222]
24. Camus V, Stamatoullas A, Mareschal S, Viailly PJ, Sarafan-Vasseur N, Bohers E, et al. Detection and prognostic value of recurrent exportin 1 mutations in tumor and cell-free circulating DNA of patients with classical Hodgkin lymphoma. Haematologica. 2016;101:1094–101. [PubMed: 27479820]
25. Lin DC, Hao JJ, Nagata Y, Xu L, Shang L, Meng X, et al. Genomic and molecular characterization of esophageal squamous cell carcinoma. Nat Genet. 2014;46:467–73. [PubMed: 24686850]
26. Chang MT, Asthana S, Gao SP, Lee BH, Chapman JS, Kandoth C, et al. Identifying recurrent mutations in cancer reveals widespread lineage diversity and mutational specificity. Nat Biotechnol. 2016;34:155–63. [PubMed: 26619011]
27. Chang MT, Bhattarai TS, Schram AM, Bielski CM, Donoghue MTA, Jonsson P, et al. Accelerating Discovery of Functional Mutant Alleles in Cancer. Cancer discovery. 2018;8:174–83. [PubMed: 29247016]
28. Hurwitz R, Hozier J, LeBien T, Minowada J, Gajl-Peczalska K, Kubonishi I, et al. Characterization of a leukemic cell line of the pre-B phenotype. Int J Cancer. 1979;23:174–80. [PubMed: 83966]
29. Wang T, Birsoy K, Hughes NW, Krupczak KM, Post Y, Wei JJ, et al. Identification and characterization of essential genes in the human genome. Science. 2015;350:1096–101. [PubMed: 26472758]
30. Blomen VA, Majek P, Jae LT, Bigenzahn JW, Nieuwenhuis J, Staring J, et al. Gene essentiality and synthetic lethality in haploid human cells. Science. 2015;350:1092–6. [PubMed: 26472760]
31. Adams JM, Harris AW, Pinkert CA, Corcoran LM, Alexander WS, Cory S, et al. The c-myc oncogene driven by immunoglobulin enhancers induces lymphoid malignancy in transgenic mice. Nature. 1985;318:533–8. [PubMed: 3906410]
32. Ogilvy S, Metcalf D, Print CG, Bath ML, Harris AW, Adams JM. Constitutive Bcl-2 expression throughout the hematopoietic compartment affects multiple lineages and enhances progenitor cell survival. Proc Natl Acad Sci U S A. 1999;96:14943–8. [PubMed: 10611317]
33. Durham BH, Getta B, Dietrich S, Taylor J, Won H, Bogenberger JM, et al. Genomic analysis of hairy cell leukemia identifies novel recurrent genetic alterations. Blood. 2017;130:1644–8. [PubMed: 28801450]
34. Fornerod M, Ohno M, Yoshida M, Mattaj IW. CRM1 is an export receptor for leucine-rich nuclear export signals. Cell. 1997;90:1051–60. [PubMed: 9323133]
35. Monecke T, Guttler T, Neumann P, Dickmanns A, Gorlich D, Ficner R. Crystal structure of the nuclear export receptor CRM1 in complex with Snurportin1 and RanGTP. Science. 2009;324:1087–91. [PubMed: 19389996]
36. Dong X, Biswas A, Suel KE, Jackson LK, Martinez R, Gu H, et al. Structural basis for leucine-rich nuclear export signal recognition by CRM1. Nature. 2009;458:1136–41. [PubMed: 19339969]

37. Guttler T, Madl T, Neumann P, Deichsel D, Corsini L, Monecke T, et al. NES consensus redefined by structures of PKI-type and Rev-type nuclear export signals bound to CRM1. Nat Struct Mol Biol. 2010;17:1367–76. [PubMed: 20972448]
38. Fung HY, Fu SC, Chook YM. Nuclear export receptor CRM1 recognizes diverse conformations in nuclear export signals. Elife. 2017;6.
39. Prieto G, Fullaondo A, Rodriguez JA. Prediction of nuclear export signals using weighted regular expressions (Wregex). Bioinformatics. 2014;30:1220–7. [PubMed: 24413524]
40. Garcia-Santisteban I, Arregi I, Alonso-Marino M, Urbaneja MA, Garcia-Vallejo JJ, Banuelos S, et al. A cellular reporter to evaluate CRM1 nuclear export activity: functional analysis of the cancer-related mutant E571K. Cell Mol Life Sci. 2016;73:4685–99. [PubMed: 27312238]
41. Henderson BR, Eleftheriou A. A comparison of the activity, sequence specificity, and CRM1-dependence of different nuclear export signals. Exp Cell Res. 2000;256:213–24. [PubMed: 10739668]
42. Hu B, Patel KP, Chen HC, Wang X, Wang F, Luthra R, et al. Routine sequencing in CLL has prognostic implications and provides new insight into pathogenesis and targeted treatments. Br J Haematol. 2019;185:852–64. [PubMed: 30924136]
43. Thakar K, Karaca S, Port SA, Urlaub H, Kehlenbach RH. Identification of CRM1-dependent Nuclear Export Cargos Using Quantitative Mass Spectrometry. Molecular & cellular proteomics : MCP. 2013;12:664–78. [PubMed: 23242554]
44. Kirli K, Karaca S, Dehne HJ, Samwer M, Pan KT, Lenz C, et al. A deep proteomics perspective on CRM1-mediated nuclear export and nucleocytoplasmic partitioning. Elife. 2015;4.
45. Wuhr M, Guttler T, Peshkin L, McAlister GC, Sonnett M, Ishihara K, et al. The Nuclear Proteome of a Vertebrate. Curr Biol. 2015;25:2663–71. [PubMed: 26441354]
46. Bahlis NJ, Sutherland H, White D, Sebag M, Lentzsch S, Kotb R, et al. Selinexor plus low-dose bortezomib and dexamethasone for patients with relapsed or refractory multiple myeloma. Blood. 2018;132:2546–54. [PubMed: 30352784]
47. Kuhn R, Schwenk F, Aguet M, Rajewsky K. Inducible gene targeting in mice. Science. 1995;269:1427–9. [PubMed: 7660125]
48. Hayashi S, McMahon AP. Efficient recombination in diverse tissues by a tamoxifen-inducible form of Cre: a tool for temporally regulated gene activation/inactivation in the mouse. Dev Biol. 2002;244:305–18. [PubMed: 11944939]
49. Moran-Crusio LR K, Shih A, Abdel-Wahab O, Ndiaye-Lobry D, Lobry C, Figueroa ME, Vasanthakumar A, Patel J, Zhao X,. Tet2 loss leads to increased hematopoietic stem cell self-renewal and myeloid transformation. Cancer Cell. 2011;20:11–24. [PubMed: 21723200]
50. Kudo N, Matsumori N, Taoka H, Fujiwara D, Schreiner EP, Wolff B, et al. Leptomycin B inactivates CRM1/exportin 1 by covalent modification at a cysteine residue in the central conserved region. Proc Natl Acad Sci U S A. 1999;96:9112–7. [PubMed: 10430904]

Significance

Here we identify that heterozygous mutations in the main nuclear exporter in eukaryotic cells, XPO1, are positively selected in cancer and promote the initiation of clonal B-cell malignancies. XPO1 mutations alter nuclear export signal recognition in a sequence-specific manner and sensitize cells to compounds in clinical development inhibiting XPO1 function.

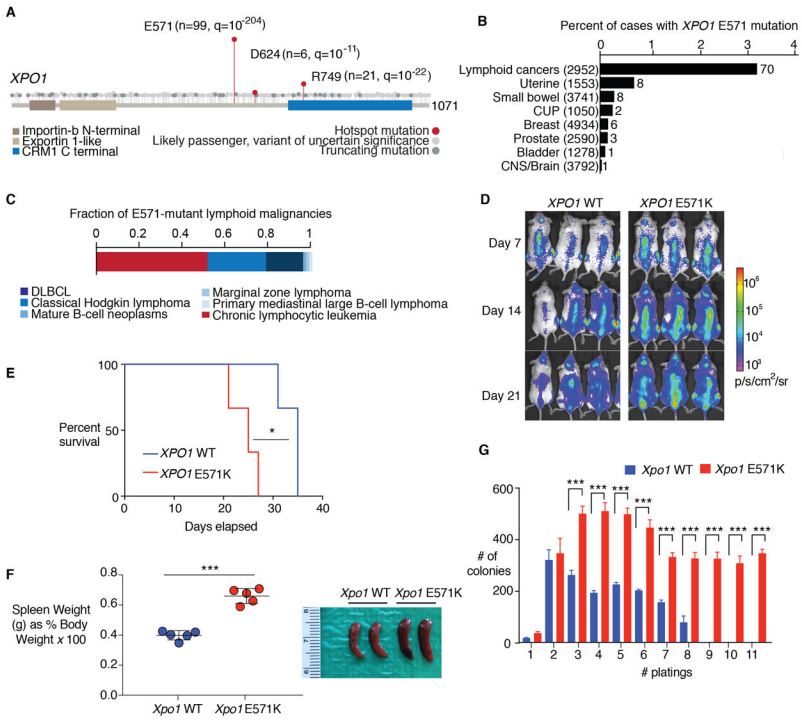

Figure 1. *XPO1* hotspot mutations promote proliferation *in vivo.*

A, Lollipop plot of the distribution and frequency of *XPO1* mutations across cancer patients and identification of statistically significant *XPO1* mutational hotspots (false discovery rate < 1%). **B,** Frequency of *XPO1* E571 mutations by cancer type in 42,793 sequenced tumors (CNS = central nervous system; CUP = cancer of unknown primary). The number of individual patients with *XPO1* E571 mutations within each disease category is also shown. **C,** Fraction of *XPO1* E571 mutations by subtype of lymphoid malignancy (DLBCL = diffuse large B-cell lymphoma). **D,** Imaging of luciferase-labeled *XPO1* WT and E571K mutant NALM-6 cells *in vivo* after xenografting into NSG mice. Four NSG mice were engrafted in each group. **E,** Kaplan-Meier survival curves of the mice from (D). Survival was computed using the Kaplan-Meier estimator (**P* = 0.02). **F,** Spleen weights and representative photos from *CD19*-cre *Xpo1*$^{WT/WT}$ and *CD19*-cre *Xpo1*$^{E571K/WT}$ mice (*n* = 5 mice/group; ruler represents centimeters). **G,** Number of colonies of bone marrow cells from *Xpo1*^{WT} and *Xpo1*$^{E571K/WT}$ mice in methylcellulose media containing IL-7 (*n* = 3 mice/group). Equal numbers of cells were replated. Differences were calculated using a two-sided Student's t-test. **P* < 0.05, ***P* < 0.01, ****P* < 0.001.

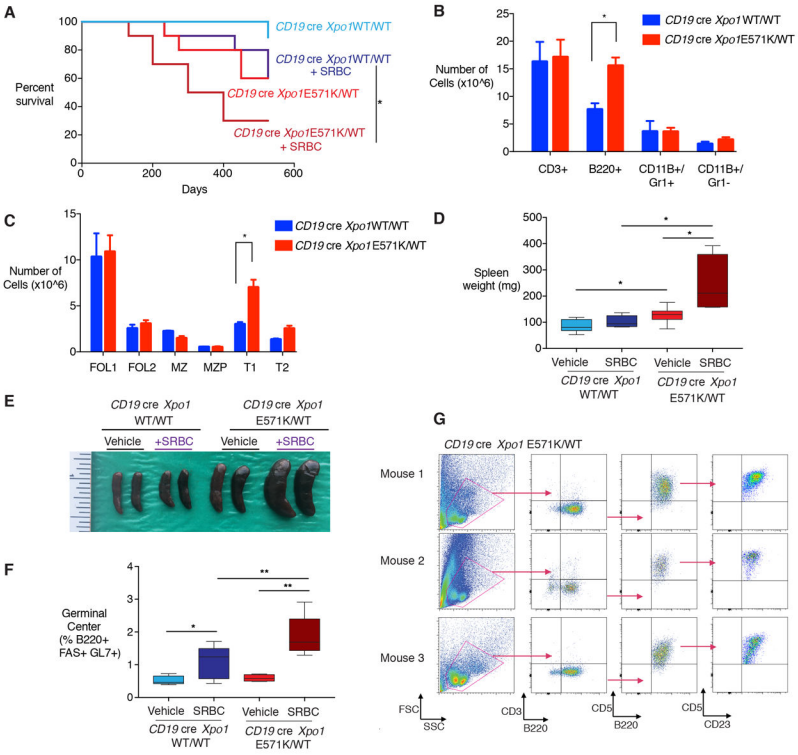

Figure 2. Endogenous expression of *Xpo1* E571K mutation in mice enhances proliferation and promotes B-cell transformation.

A, Kaplan-Meier survival curve of *CD19*-cre Xpo1$^{WT/WT}$ and *CD19*-cre *Xpo1*$^{E571K/WT}$ mice treated monthly with vehicle or allo-immunization with sheep red blood cells (SRBC; $n = 10$ mice/group). **B,** Number of mature myeloid and lymphoid cells in the bone marrow and **C,** B-cell subsets in spleens of 12-week-old *CD19*-cre *Xpo1*$^{WT/WT}$ ($n = 5$ mice) and *CD19*-cre *Xpo1*$^{E571K/WT}$ mice ($n = 5$ mice) (MZ = marginal zone [CD19$^+$ CD21^{hi} IgM^{hi} B220$^+$ CD23$^-$]; MZP = marginal zone precursor [CD19$^+$ CD21^{hi} IgM^{hi} B220$^+$ CD23$^-$]; FOL = follicular [CD19$^+$ CD21$^+$ IgM$^+$ IgD$^+$], T = transitional [CD19$^+$ CD21^{lo} IgM^{hi} CD93$^+$]). **D,** Spleen weights and **E,** representative images of spleens at time of death from mice in (A) (ruler represents inches). **F,** Frequency of germinal center (B220$^+$ FAS$^+$ GL7$^+$) B-cells in spleens from *CD19*-cre *Xpo1*$^{E571K/WT}$ or *CD19*-cre *Xpo1*$^{WT/WT}$ mice one week after SRBC or vehicle treatment ($n = 7$ mice/group). **G,** Flow cytometry of tumors from three independent *CD19*-cre *Xpo1*$^{E571K/WT}$ mice showing B220/CD5/CD23 triple-positive cells in peripheral blood. Differences were calculated using a two-sided Student's t-test. *$P < 0.05$, **$P < 0.01$.

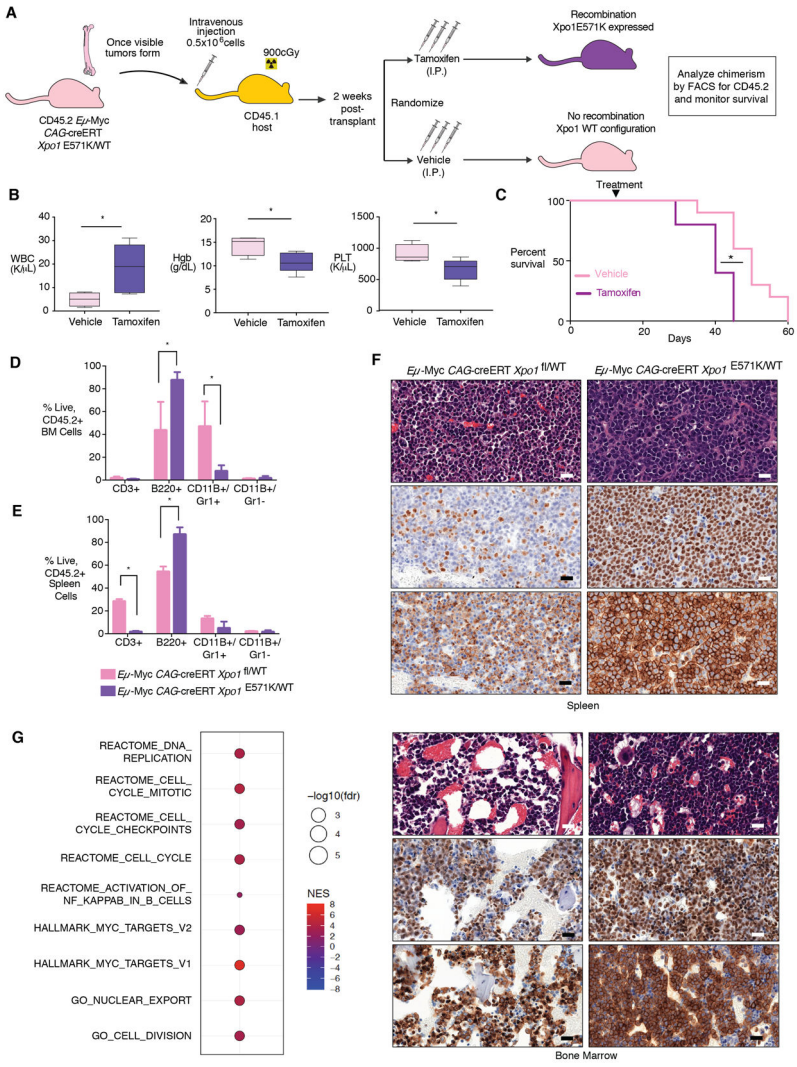

Figure 3. *Xpo1* mutations cooperate with MYC overexpression to drive lymphomagenesis.

A, Schema of the method to analyze the effect of the *Xpo1* E571K mutation on MYC-driven B-cell lymphomagenesis *in vivo*. *CAG*-creERT *Xpo1*$^{E571K/WT}$ *Eμ*-Myc mice were generated on a CD45.2 C57BL/6J mice background and then 1×10^6 bone marrow (BM) mononuclear cells were transplanted into lethally irradiated CD45.1 C57BL/6J recipient mice. Following 2 weeks of engraftment, tamoxifen was administered intraperitoneally (I.P.) to half of the recipients to result in expression of the mutant allele while vehicle was administered to the other half of the recipients. **B,** Complete blood counts (WBC = white blood cells; Hgb = hemoglobin; PLT = platelets) from *CAG*-creERT *Xpo1*$^{E571K/WT}$ *Eμ*-Myc mice with (tamoxifen) or without (vehicle) induction of the *Xpo1*$^{E571K/WT}$ at end-stage disease (n = 5 recipient mice/group). **C,** Kaplan-Meier survival curves of recipients of BM from *CAG*-creERT *Xpo1*$^{E571K/WT}$ *Eμ*-Myc following tamoxifen or vehicle treatment resulting in expression of *Xpo1* mutant allele or *Xpo1* wild-type configuration respectively (n = 5 mice/group). Number of mature myeloid and lymphoid cells in the **D,** BM and **E,** spleen of recipients of mice from (C) at end-stage disease (n = 5 recipient mice/group). **F,** Hematoxyiln and eosin stain (top), anti-Ki67 immunohistochemical (IHC) stain (middle),

and anti-B220 IHC stain (bottom) in spleen (first three rows) and bone marrow (bottom three rows) from *CAG*-creERT *Xpo1*$^{WT/WT}$ *Eμ*-Myc and *CAG*-creERT *Xpo1*$^{E571K/WT}$ *Eμ*-Myc mice. Scale bars: 100 μm (left) and 20 μm (right). **G,** Gene ontology analysis for biological processes significantly enriched in differentiatlly expressed genes from mRNA sequencing of *CAG*-creERT *Xpo1*$^{E571K/WT}$ *Eμ*-Myc versus *CAG*-creERT *Xpo1*$^{WT/WT}$ *Eμ*-Myc tumors. (FDR: False Discovery Rate; NES: Normalized Enrichment Score). Survival was computed using the Kaplan-Meier estimator. Differences were calculated using a two-sided Student's t-test, $*P < 0.05$.

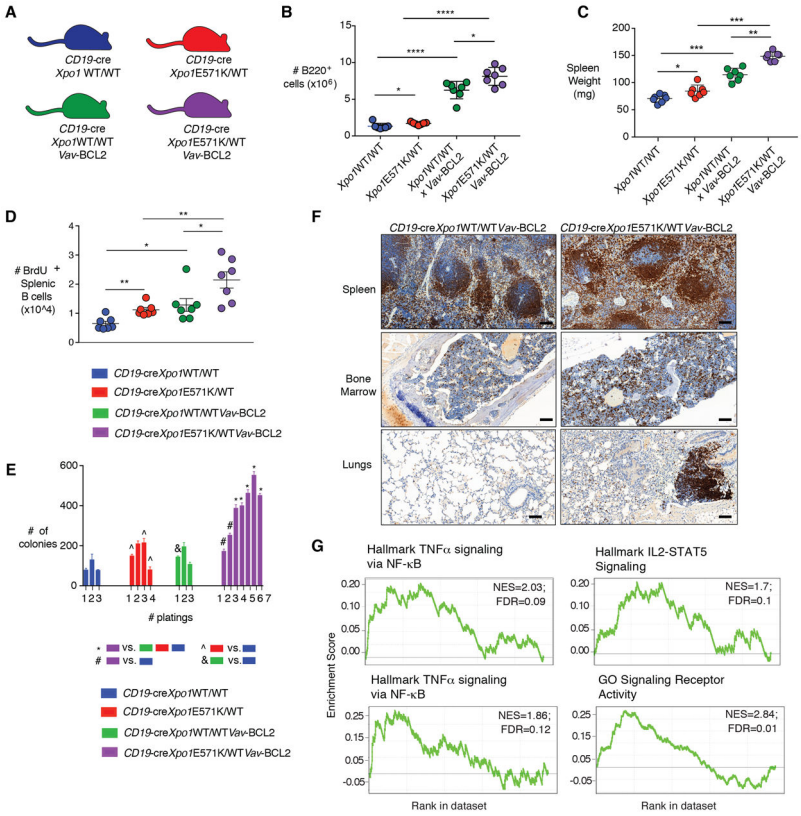

Figure 4: *Xpo1* mutations cooperate with BCL2 overexpression to drive lymphomagenesis.

A, Schematic showing the four genotypes of mice created by crossing *CD19*-cre *Xpo1*$^{E571K/WT}$ and *Vav*-BCL2 mice. **B,** Absolute number of B-cells in the peripheral blood and **C,** spleen weight of 12-week-old *CD19*-cre *Xpo1*$^{WT/WT}$, *CD19*-cre *Xpo1*$^{E571K/WT}$, *CD19*-cre *Xpo1*$^{WT/WT}$ *Vav*-BCL2, and *CD19*-cre *Xpo1*$^{E571K/WT}$ *Vav*-BCL2 mice ($n = 7$ mice/group). **D,** Number of BrdU^{+} (bromodeoxyuridine) splenic B220^{+} B-cells from 12-week-old mice (BrdU was administered *in vivo* and animals sacrificed 48 hours later for analysis). **E,** Number of colonies grown from BM cells from respective genotypes in IL-7 containing methylcellulose. **F**, Anti-B220 immunohistochemistry in *CD19*-cre *Xpo1*$^{WT/WT}$ *Vav*-BCL2 and *CD19*-cre *Xpo1*$^{E571K/WT}$ *Vav*-BCL2 mice. Scale bars: 200 μm **G,** Gene set enrichment analysis of key pathways dysregulated from mRNA sequencing of *CD19*-cre *Xpo1*$^{E571K/WT}$ *Vav*-BCL2 versus *CD19*-cre *Xpo1*$^{WT/WT}$ *Vav*-BCL2 mice (FDR: False Discovery Rate; NES: Normalized Enrichment Score). Differences were calculated using a two-sided Student's t-test, $*P < 0.05$, $**P < 0.01$, $***P < 0.001$, $****P < 0.0001$.

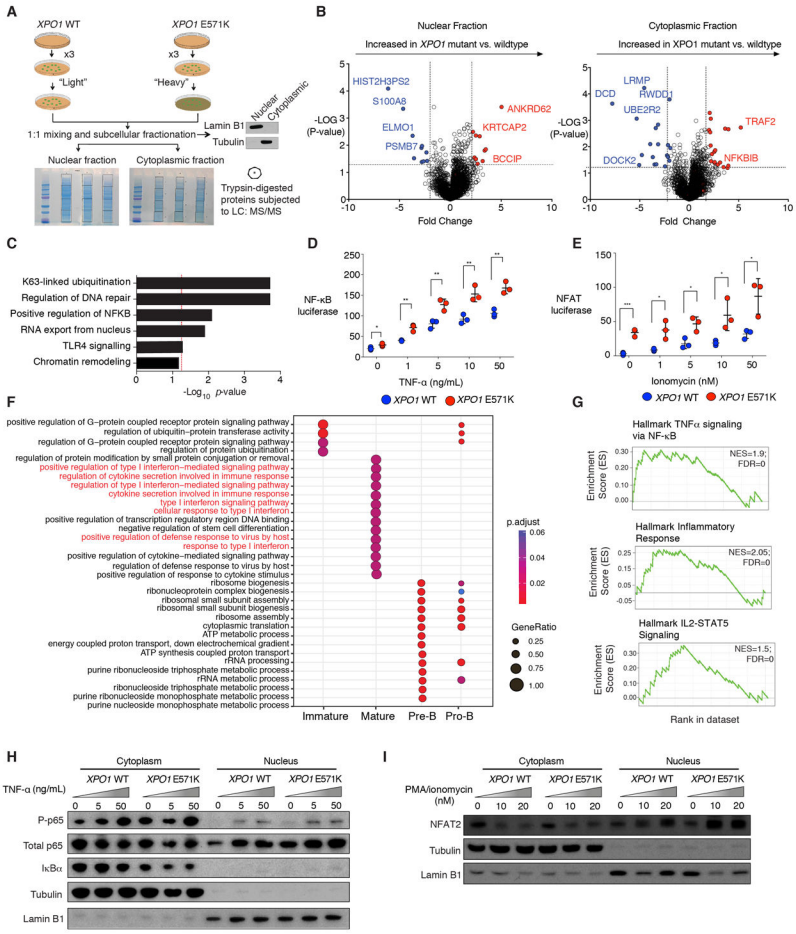

Figure 5. Aberrant nuclear/cytoplasmic compartmentalization of proteins and enhanced immune signaling in *XPO1* mutant cells.

A, Schema of SILAC (stable isotope labeling of amino acids in culture)-based mass spectrometry analysis of nuclear and cytoplasmic proteins from isogenic NALM-6 *XPO1*$^{E571K/WT}$ and *XPO1*$^{WT/WT}$ cells. SILAC experiments were performed in biological triplicate. **B,** Volcano plots of differential protein abundance in *XPO1*$^{E571K/WT}$ compared to *XPO1*$^{WT/WT}$ cells in nucleus (left) and cytoplasm (right) from experiment in (A). X-axis represents fold-change with dotted lines indicating fold change ratios = |2| and Y-axis represents significance with dotted lines at –log$_{10}$[*P*-value] of 1.30. **C,** Enrichment analysis of proteins mislocalized in *XPO1* mutant relative to WT cells from (B) (red line indicates pathways with significant enrichment at –log$_{10}$[*P*-value] of 1.30). **D,** Quantification of NF-κB luciferase reporter activity after stimulation of cells with TNF-α, and **E,** NFAT luciferase reporter activity after stimulation with PMA/ionomycin. Differences were calculated using a two-sided Student's t-test. **P* < 0.05, ***P* < 0.01, ****P* < 0.001. **F,** Gene ontology analysis for biological processes significantly enriched in *CD19*-cre *Xpo1*$^{E571K/WT}$ versus *CD19*-cre *Xpo1*$^{WT/WT}$ mice across several subpopulations of B cells. **G,** Gene set enrichment analysis of key pathways dysregulated from RNA-seq of CLL patients with or without *XPO1* E571K mutations ("NES" in this case represents the normalized enrichment score). **H,** Western blot of nuclear and cytoplasmic P-p65 and IκBα after stimulation of XPO1 mutant or WT cells

with two doses of TNFα. **I,** Western blot of nuclear NFAT2 after stimulation of XPO1 mutant or WT cells with PMA and two doses of ionomycin.

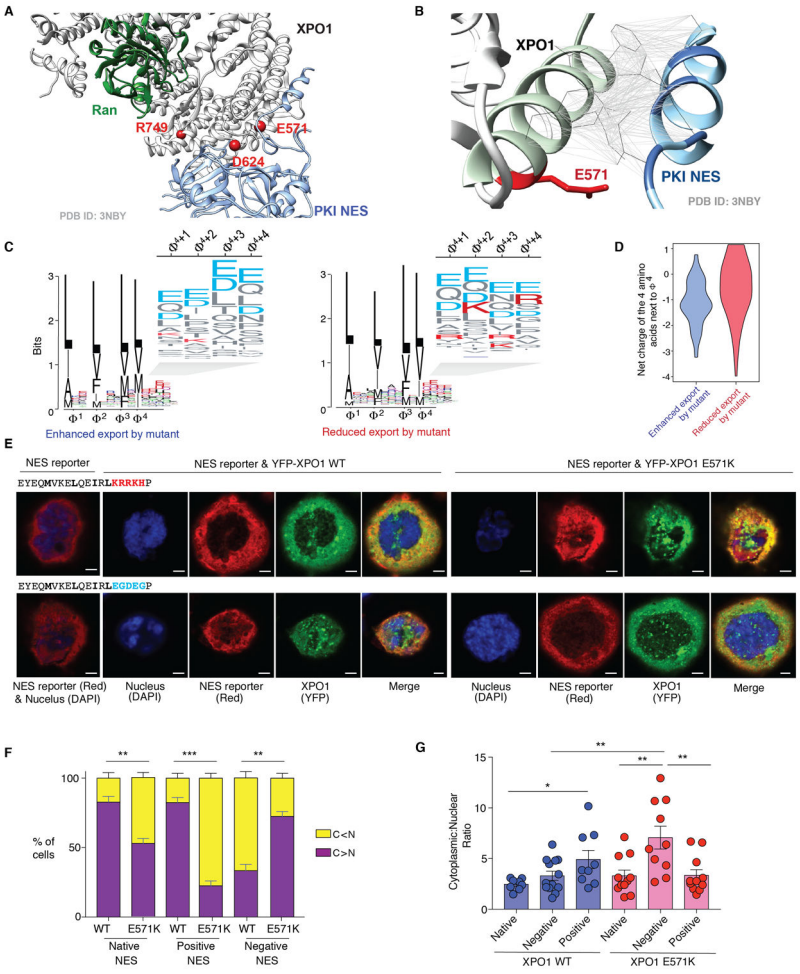

Figure 6. *XPO1* mutations alter nuclear export of cargo proteins based on the charge of amino acids C-terminal to their nuclear export signal (NES).

A, Structure of XPO1 (gray) in complex with a protein cargo (protein kinase inhibitor [PKI]; in blue) having a classical NES (structure as previously published (37)). In green is the GTP-binding nuclear protein Ran, while the position of the two tumor-specific XPO1 hotspot mutations (E571 and D624) are labeled in red. **B,** In light green is the helix of XPO1 (gray) from which mutant E571 (red) directly interacts with the classical NES sequence (LALKLAGLDI) of the protein cargo (PKI; light blue). Critical hydrophobic positions on the cargo required for interactions with XPO1 are colored dark blue and shown as wireframes along with those interacting XPO1 residues. Gray lines show the hydrophobic interactions XPO1 and PKI. **C,** Sequence logos illustrating the amino acid residue content of putative NESs predicted in proteins differentially exported in *XPO1* mutant relative to wild-type (WT) cells from the experiment in Figure 4A. $\Phi^{1\text{-}4}$ indicate the four hydrophobic amino acid positions (consisting of leucine, isoleucine, valine, phenylalanine, or methionine) in the consensus NES of XPO1 cargo proteins. Insets show the four amino acids C-terminal to the last hydrophobic amino acid residue within the NES (negatively charged residues shown in blue; positively charged residues shown in red). **D,** Violin plots quantifying the net charge of the four amino acids following Φ^4 in proteins with enhanced versus reduced export in cells

expressing the XPO1 E571K mutation. **E,** Confocal microscopy images of cells expressing YFP-*XPO1*^{WT} (left three panels) or YFP-*XPO1*$^{E571K/WT}$ (right three panels) constructs with a nuclear export reporter plasmid bearing IκBα NES mutagenized to possess either a positively (top) or negatively (bottom) charged C-terminal end (reporters alone on far left panels). Of note, the function of transfected XPO1 E571K or XPO1 WT was evaluated in isolation from endogenous XPO1 in these experiments as cells were exposed to the XPO1 inhibitor leptomycin B and both XPO1 WT and E571K cDNAs also contained the C528S mutation (a mutation conferring resistance to leptomycin B (50); see Supplementary Figure S6D). Scale bar: 5 μm. **F,** Ratio of enhanced (purple) or reduced (yellow) nuclear export of IκBα NES reporter in each condition from (B) (where "C" represents cytoplasmic localization of the reporter and "N" nuclear localization of the reporter). Bars represent an average of measurements of 10-12 cells by two independent assessments with error bars representing the standard deviation between assessments. **G,** Mean cytoplasmic to nuclear ratio of intensity of IκBα NES reporter signal in each condition from (B) as measured by image analysis software. Individual points represent cytoplasmic to nuclear ratio and error bars represent standard deviation. $*P < 0.05$, $**P < 0.01$. Quantification of differences were calculated using a two-sided Student's t-test.

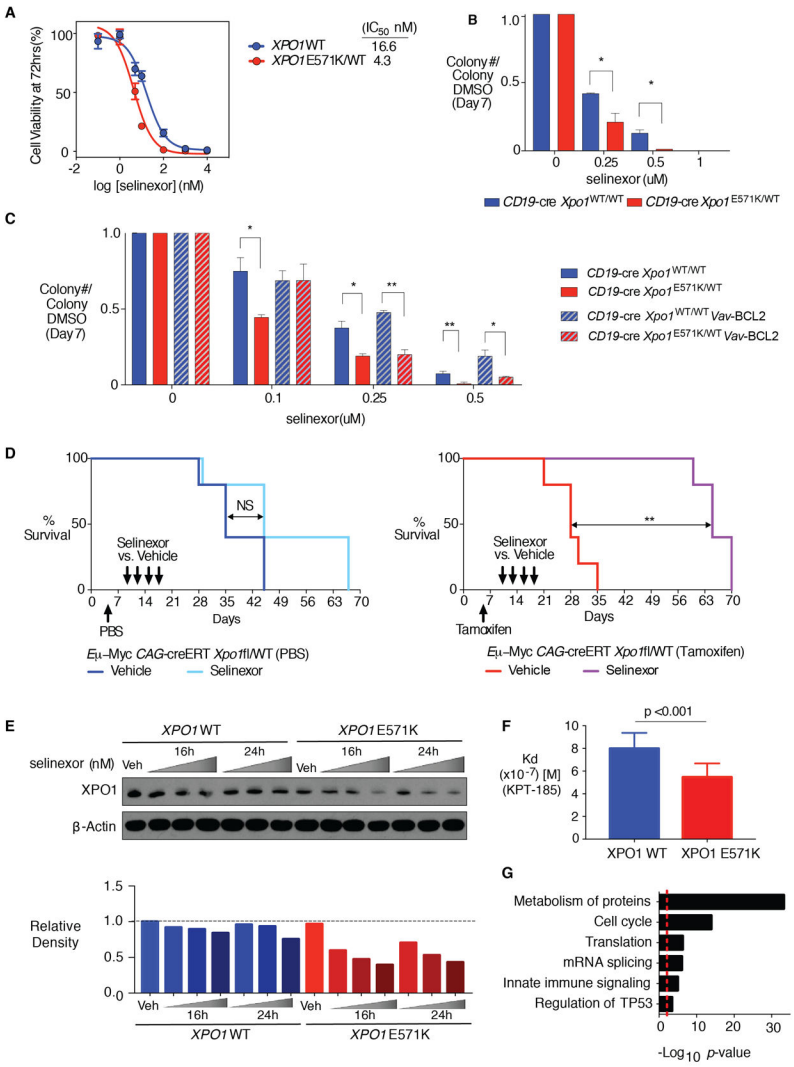

Figure 7. Enhanced sensitivity of XPO1 mutant cells to XPO1 inhibition *in vitro* and *in vivo*.

A, Dose response curve and IC_{50} values of isogeneic NALM-6 *XPO1*^{WT} or *XPO1*$^{E571K/WT}$ cell lines treated with selinexor. **B,** Number of colonies from bone marrow mononuclear cells (BM MNCs) from C*D19*-cre Xpo1$^{WT/WT}$ and *Xpo1*$^{E571K/WT}$ mice grown in IL-7 containing methylcellulose with either vehicle (DMSO) or increasing doses of KPT-330. Bar graphs represent the number of colonies with each treatment relative to vehicle controls. **C,** Number of colonies from BM MNCs from *Vav*-BCL2 *CD19*-cre *Xpo1*$^{WT/WT}$ or *Vav*-BCL2 *CD19*-cre *Xpo1*$^{E571K/WT}$ knock-in mice treated with either vehicle (DMSO) or selinexor. **D,** Kaplan-Meier curves of *CAG*-creERT *Xpo1*$^{E571K/WT}$ *Eμ*-Myc mice without induction of the *Xpo1*$^{E571K/WT}$ mutation (left) or with induction of the mutation (tamoxifen; right) treated with selinexor or vehicle. **E,** XPO1 protein levels by western blot (top; quantification below) in NALM-6 *XPO1*^{WT} or *XPO1*$^{E571K/WT}$ cell lines treated with selinexor for 16 or 24 hours (5, 10 and 50nM doses). **F,** Bar plots of cell free, *in vitro* binding affinity (Kd) values of the binding of KPT-185 to purified XPO1 wild-type or XPO1 E571K protein. **G,** Gene ontology analysis of proteins retained in the nucleus in *XPO1*$^{E571K/WT}$ cells relative to wild-type after XPO1 inhibition (red line indicates pathways with significant enrichment at $-\log_{10}$[*P*-value]

of 1.30). Differences were calculated using a two-sided Student's t-test. *$P < 0.05$, ** $P < 0.01$.